Hibler, D. W., Stolowich, N. J., Reynolds, M. A., Gerlt, J. A., Welde, J. A., & Bolton, P. H. (1987) *Biochemistry 26*, 6278.
Higgins, W., Fairwell, T., & Miles, E. W. (1979) *Biochemistry 18*, 4827.
Hurle, M. R. (1987) Ph.D. Thesis, The Pennsylvania State University.
Hurle, M. R., & Matthews, C. R. (1987) *Biochim. Biophys. Acta 913*, 179.
Hurle, M. R., Michelotti, G. A., Crisanti, M. M., & Matthews, C. R. (1987) *Proteins: Struct., Funct., Genet. 2*, 54.
Hyde, C. C., Ahmed, S. A., Padlan, E. A., Miles, E. W., & Davies, D. R. (1988) *J. Biol. Chem. 263*, 17857.
Kirschner, K., Wiskocil, R. L., Foehn, M., & Rezeau, L. (1975) *Eur. J. Biochem. 60*, 513.
Luger, K., Hommel, U., Herold, Hofsteenge, J., & Kirschner, K. 1989) *Science 243*, 206.
Marqusee, S., & Baldwin, R. L. (1987) *Proc. Natl. Acad. Sci. U.S.A. 84*, 8998.
Matthews, C. R. (1987) *Methods Enzymol. 154*, 498.
Matthews, C. R., & Crisanti, M. M. (1981) *Biochemistry 20*, 784.
Matthews, C. R., Cristanti, M. M., Manz, J. T., & Gepner, G. L. (1983) *Biochemistry 22*, 1445.
Miles, E. W., Yutani, K., & Ogasahara, K. (1982) *Biochemistry 21*, 2586.
Murgola, E. J., & Yanofsky, C. (1974) *J. Mol. Biol. 86*, 775.
Oas, T. G., & Kim, P. S. (1988) *Nature 336*, 42.
Perry, K. M., Onuffer, J. J., Touchette, N. A., Herndon, C. S., Gittelman, M. S., Matthews, C. R., Chen, J. T., Mayer, R. J., Taira, K., Benkovic, S. J., Howell, E. E., & Kraut, J. (1987) *Biochemistry 26*, 2674.
Privalov, P. L. (1986) *J. Mol. Biol. 190*, 487.
Privalov, P. L., & Gill, S. (1988) *Adv. Protein Chem. 39*, 191.
Roder, H., Elove, G. A., & Englander, S. W. (1988) *Nature 335*, 700.
Schellman, J. A. (1978) *Biopolymers 17*, 1305.
Udgaonkar, J. B., & Baldwin, R. L. 1988) *Nature 335*, 694.
Yanofsky, C., Berger, H., & Brammar, W. J. (1969) *Proc. Int. Congr. Genet., 12th 3*, 155.

Solution Structural Characterization of Cyanometmyoglobin: Resonance Assignment of Heme Cavity Residues by Two-Dimensional NMR†

S. Donald Emerson and Gerd N. La Mar*
Department of Chemistry, University of California, Davis, California 95616
Received June 6, 1989; Revised Manuscript Received September 11, 1989

ABSTRACT: Steady-state nuclear Overhauser effects (NOE), two-dimensional (2D) nuclear Overhauser effect spectroscopy (NOESY), and 2D spin correlation spectroscopy (COSY) have been applied to the fully paramagnetic low-spin, cyanide-ligated complex of sperm whale ferric myoglobin to assign the majority of the heme pocket side-chain proton signals and the remainder of the heme signals. It is shown that the 2D NOESY map reveals essentially all dipolar connectivities observed in ordinary 1D NOE experiments and expected on the basis of crystal coordinates, albeit often more weakly than in a diamagnetic analogue. For extremely broad (~600-Hz) and rapidly relaxing ($T_1 \sim 3$ ms) signals which show no NOESY peaks, we demonstrate that conventional steady-state NOEs obtained under very rapid pulsing conditions still allow detection of the critical dipolar connectivities that allow unambiguous assignments. The COSY map was found to be generally less useful for the hyperfine-shifted residues, with cross peaks detected only for protons >6 Å from the iron. Nevertheless, numerous critical COSY cross peaks between strongly hyperfine-shifted peaks were resolved and assigned. In all, 95% (53 of 56 signals) of the total proton sets within ~7.5 Å of the iron, the region experiencing the strongest hyperfine shifts and paramagnetic relaxation, are now unambiguously assigned. Hence it is clear that the 2D methods can be profitably applied to paramagnetic proteins. The scope and limitations of such application are discussed. The resulting hyperfine shift pattern for the heme confirmed expectations based on model compounds. In contrast, while exhibiting fortuitous ^{1}H NMR spectral similarities, a major discrepancy was uncovered between the hyperfine shift pattern of the axially bound (F8 histidyl) imidazole in the protein and that of the imidazole in a relevant model compound [Chacko, V. P., & La Mar, G. N. (1982) *J. Am. Chem. Soc. 104*, 7002–7007], providing direct evidence for a protein-based deformation of axial bonding in the protein.

Myoglobin (Mb)[1] is a small (~16-kDa) hemoprotein whose function in tissue is to reversibly bind molecular oxygen, which it carries out with remarkable variability with genetic origin of the polypeptide chain. Mb can exist in both the reduced iron(II) state as well as oxidized iron(III) state, and both the diamagnetic and paramagnetic derivatives have been the subject of intense physicochemical studies to elucidate the mechanism of control of ligand binding (Antonini & Brunori, 1971). The wide study of hemoproteins in general is due, in large part, to the ability to compare properties of not only diverse genetic variants but also the intact protein with the extracted prosthetic group (i.e., model compounds), thereby

†This research has been supported by a grant from the National Institutes of Health (HL16087).

[1] Abbreviations: Mb, myoglobin; metMbCN, cyanide-ligated ferric myoglobin; NOE, nuclear Overhauser effect; DSS, 2,2-dimethyl-2-silapentane-5-sulfonate; NOESY, two-dimensional nuclear Overhauser effect spectroscopy; COSY, two-dimensional correlation spectroscopy; DQF-COSY, double-quantum-filtered COSY.

0006-2960/90/0429-1545$02.50/0

providing detailed information on the mechanism of control of function by the polypeptide chain. Moreover, sperm whale Mb in particular is frequently studied as a prototype biopolymer on which to test the scope and limitation of new physical and theoretical advances in biophysics (Case & Karplus, 1979; Karplus & McCammon, 1981; Debrunner & Frauenfelder, 1982; Gelin et al., 1983). The recent successful expression in *Escherichia coli* of numerous point mutants of sperm whale Mb based on a synthetic gene further expands the important role of this protein in the development of our detailed understanding of the correlation of function with protein structure and dynamics (Springer et al., 1989; Perutz, 1989).

Nuclear magnetic resonance (NMR) constitutes one of the major tools for elucidating the solution structure of proteins (Wüthrich, 1986), and significant molecular structural details have been been derived for diamagnetic Mb complexes (MbCO, MbO_2). While the stereochemical structural information content of paramagnetic derivatives may be lower than in diamagnetic complexes, the hyperfine shifts provide unique additional information on the electronic/magnetic properties of the heme that are inaccessible in diamagnetic systems (La Mar, 1979; Satterlee, 1985). There are compelling reasons for such detailed ^1H NMR studies on a well-understood paramagnetic protein, since many hemoproteins, as well as other metalloproteins, exist only in paramagnetic functional states. Considerable effort has been expended toward characterization of the NMR spectra of paramagnetic heme model compounds (La Mar & Walker, 1979), and until recently, such comparisons constituted one of the major bases for assignment of resonances in intact proteins (La Mar, 1979). In general, it has been concluded that the hyperfine shift pattern in models and proteins reflects very similar electronic structure of the iron–prophyrin and iron–axial ligand bonding, except that the heme in-plane asymmetry in the protein environment is larger (Shulman et al., 1971; La Mar, 1979; Satterlee, 1985).

The information content of hyperfine shifts in low-spin ferric hemoproteins is extremely rich, since this state exhibits both contact and dipolar shifts (Shulman et al., 1971; Jesson, 1973; La Mar, 1979; Satterlee, 1985). The contact shift provides details of the covalent bonds to the iron (La Mar, 1973), while the dipolar shift provides both molecular structural details for noncoordinated amino acid residues and information on the magnetic properties of the iron (Shulman et al., 1971; Horrocks, 1973). Preliminary NMR data on synthetic mutants (K. Rajarathnam, G. N. La Mar, M. Chiu, and S. G. Sligar, unpublished results) as well as natural variants (Wüthrich et al., 1970; Krishnamoorthi et al., 1984) of mammalian Mb can show dramatic changes in hyperfine shift patterns even when diamagnetic MbCO NMR shifts are only slightly perturbed. This wealth of information in the hyperfine shift, however, becomes accessible only upon first unambiguously assigning the hyperfine-shifted resonances and, second, upon effecting the quantitative factoring of the dipolar and contact contributions to the shifts (Jesson, 1973; Horrocks, 1973). In this report, we consider the prospects for implementing the needed assignments. Similarly extensive assignments have been reported to date only for ferricytochrome *c*, which were obtainable in the reduced, diamagnetic form by using standard 2D NMR methodology, and then transferred to the oxidized, paramagnetic protein by saturation transfer modulated by facile electron exchange (Williams et al., 1985a,b). For the protein of interest here, sperm whale metMbCN, there is no similar diamagnetic homologue, and hence the complete resonance assignments must be derived directly on the fully paramagnetic, $S = {}^1/_2$ derivative.

Partial assignment of heme resonances for sperm whale metMbCN have been reported on the basis of isotope labeling of the removable heme (Mayer et al., 1974; Sankar et al., 1987). More recently, the steady-state nuclear Overhauser effect (NOE) (Noggle & Schirmer, 1971) has resulted in the assignment of the side chains of Ile FG5 and Phe CD1 (Ramaprasad et al., 1984a; Emerson et al., 1988). Some of the exchangeable protons in the heme cavity have also been assigned, initially by analysis of differential paramagnetic-induced dipolar relaxation (Cutnell et al., 1981), and later confirmed by the steady-state NOE (Lecomte & La Mar, 1986). A tentative assignment of the critical proximal His F8 ring protons was based on the observation of similarly hyperfine-shifted and broadened resonances in model and protein (La Mar et al., 1982). The assignments, however, are very incomplete and, in the case of His F8, purely speculative, and must be confirmed.

The 2D NOE (NOESY) and spin correlation (COSY) experiments have been very successfully applied to diamagnetic MbCO (Mabbut & Wright, 1985; Dalvit & Wright, 1987). Such applications to paramagnetic derivatives, however, can present several problems. The hyperfine shifts (contact and dipolar) will obscure the useful chemical shift correlation with functional group identity. The paramagnetic-induced relaxation will both broaden lines and significantly increase the intrinsic spin–lattice relaxation rate (Swift, 1973). Thus the fast relaxation can prevent the buildup of significant NOESY cross peaks even for pairs of protons in close proximity (Macura & Ernst, 1980); the increased line width will make any given cross peak harder to detect. In the COSY experiment, increased relaxation will decrease the time for the development of coherence as well as obliterate cross peaks due to overlap, and hence cancellation of the antiphase components (Müller et al., 1986). These problems, however, influence the various protons in a paramagnetic protein in a highly differential manner. Both hyperfine shifts and paramagnetic relaxation effects are very short ranged and hence interfere with the assignments of particularly protons near the iron center. In metMbCN, protons >7.5 Å from the iron experience negligible paramagnetic relaxation and line broadening (Cutnell et al., 1981). Thus the application of 2D NOESY and COSY to these assignments should not constitute a problem, since that portion of the protein is, for all practical purposes, "diagmagnetic". The problem arises for protons <7.5 Å from the iron, for which the R_{Fe}^{-6} dependence of paramagnetic relaxation (Swift, 1973; Cutnell et al., 1981) yields T_1s as short as 4 ms and line widths as large as 600 Hz. The importance of obtaining all of the assignments of protons <7.5 Å from the iron is due to the fact that they represent precisely those residues, His F8, E7, FG3, Val E11, Phe CD1, and Ile FG5, proposed to provide the control of ligand binding (Antonini & Brunori, 1971). The stereochemistry of those and other residues in the heme cavity are depicted in Figure 1. Since 1D experiments have provided NOEs for protons with T_1s as short as 20 ms (Emerson et al., 1988), the prospects for constructive extension of 2D methods to metMbCN appear reasonable. Preliminary 2D NOESY maps for ferricytochrome b_5 have demonstrated that all of the heme resonances can be assigned (McLachlan et al., 1988).

Our goal in this report is to delineate the scope and limitations of simple 2D NOESY and COSY experiments for resonance assignments in $S = {}^1/_2$ metMbCN. An initial criterion for evaluating the NOESY map is the identification

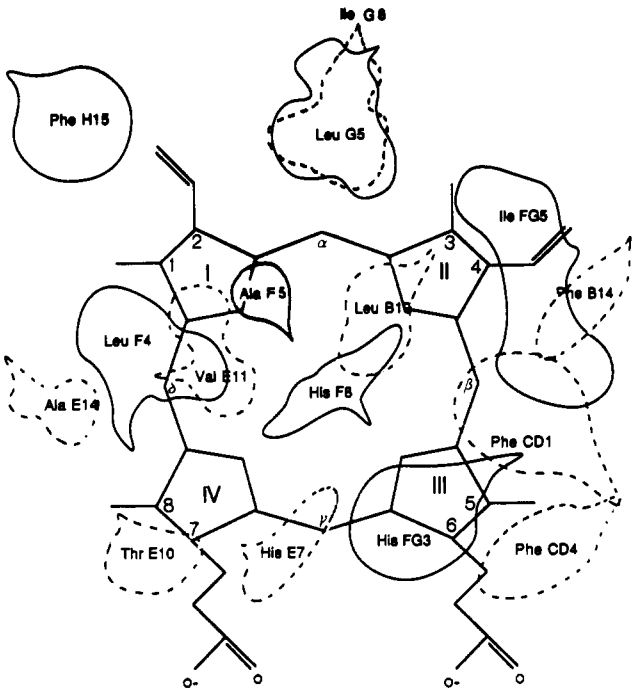

FIGURE 1: Schematic representation of the spatial disposition of amino acid side chains in the heme pocket of sperm whale Mb, as viewed face-on the heme from the proximal side. Solid and dotted lines represent the residues on the proximal and distal sides, respectively; the pointed peak of each surface indicates the location of C_α for each residue.

of not only all cross peaks that correspond to clearly observed NOEs in 1D experiments, either previously reported or performed here, but also the location of the cross peaks between identified resonances that cannot be detected by 1D means. Additional assignment aids are provided by the paramagnetic-induced dipolar relaxation, which because of the R_{Fe}^{-6} dependence, yields the distance from the iron if T_1 can be measured and are dominated by paramagnetic effects. Specifically, we set as our primary goal the assignment of all resonances <7.5 Å from the iron for residues which exhibit any resolved signal, with particular emphasis on those closest to the iron. As a secondary goal, we will search for the closest known dipolar-connected protons for those residues in contact with the heme periphery and the proximal His. While the emphasis will be to show that the desired data can be extracted from 2D maps, as many as possible for the NOESY peaks will be confirmed by 1D NOE methodology. The utility of this endeavor not only is to be measured by the information obtained for this particular protein but also can be viewed as a prototype study for applying these methods to other, less well-characterized hemoproteins (Thanabal et al., 1987a,b, 1988). The resulting hyperfine shift patterns for the heme and bound His imidazole in metMbCN will be compared with those of model compounds (Chacko & La Mar, 1982) to assess more critically the utility of model compounds for assignment purposes (La Mar, 1979; La Mar et al., 1982). In our companion report (Emerson & La Mar, 1990), we demonstrate how the experimentally determined dipolar shifts for noncoordinated residues which result from the present assignments lead to new insight into the heme–protein interactions that are the major determinants of the electronic/magnetic properties of the heme.

Materials and Methods

Preparation of Samples. Sperm whale myoglobin was purchased from Sigma Chemical Co. as a lyophilized powder and used without further purification. Cyanometmyoglobin (metMbCN) was prepared by dissolution of the lyophilate in ^2H_2O containing 0.2 M NaCl and 20 mM KCN. The sample was ultrafiltered to replace the solvent after labile proton exchange. The pH* was adjusted with 0.2 M solutions of NaO^2H and ^2HCl; reported pH* values are uncorrected for isotope effect. H_2O samples were made as described previously with the exception that all solutions were 90% in H_2O and 10% in ^2H_2O to provide the lock signal.

^1H NMR Measurements. ^1H NMR spectra were recorded on Nicolet NT-360 and NT-500 spectrometers operating in the quadrature mode at 360 and 500 MHz, respectively. The spectra of Figure 2B–D were collected by using a standard inversion–recovery pulse sequence, t–90°$_x$–240°$_y$–90°$_x$–τ–90°$_\phi$–Acq, where the relaxation delay (t) was set to 1 ms (Patt & Sykes, 1972; Eads et al., 1986). The 4096 block size and 32258-MHz spectral window gave an acquisition time of 63.5 ms. This rapid repetition rate gives significant suppression of the intense diamagnetic envelope and therefore allows optimal detection of the rapidly relaxing signals throughout the spectral window. The temperature was chosen to allow partial resolution of signals P6 and P8 from nearby methyl signals. The spectra of metMbCN in ^1H_2O in Figure 3 were collected by using a modification of the inversion–recovery pulse sequence described above, in which a decoupler saturation pulse was inserted in the τ period. The τ period, including the 200-ms decoupler saturation pulse, was adjusted to correspond with the null for the recovery of the intense ^1H_2O signal. The spectra were recorded at 30 °C to allow optimum separation between signals, P5 and P8, as well as between signals P6 and I7. The steady-state nuclear Overhauser spectra were recorded at 500 MHz by application of the 150-ms presaturation pulse with the decoupler on-resonance, with off-resonance spectra collected to provide a reference (Emerson et al., 1988). Computer difference spectra generate the fractional intensity change. Steady-state NOE difference spectra were also collected upon saturating each of the ~25 resolved resonances over the range 5–45 °C to determine the temperature dependence of all NOE-detected resonances at optimal resolution and to certify that NOEs common to two or more nonequivalent protons are not a coincidence. In all cases the NOE-detected peak could be correlated with observed NOESY cross peaks but at much better resolution for the former experiment. Only the NOESY map, which efficiently displays all information, is presented. 1D NOE spectra for the saturation of the resolved resonances not shown in the text are provided as supplementary material, with the NOEs identified by the number that corresponds to the cross peak in the NOESY and COSY maps in the text.

The phase-sensitive NOESY map shown in portions in Figures 4–6 was collected at 30 °C by using the method of States et al. (1982). The residual $^1HO^2H$ signal was suppressed by a 22-dB (0.2-W) decoupler power during the relaxation delay and mixing time. The mixing time was chosen as 50 ms, a time short enough to ensure that negligible spin diffusion takes place. The data were collected with an 8.3-μs 90° pulse over a 15625-Hz bandwidth at 360-MHz ^1H using 8192 data points; the transmitter was placed at 10.5 ppm in order to achieve optimum digital resolution across the required spectral window with our limited data arrays. A total of 320 scans per t_1, with t_1(max) = 16.4 ms, were collected with a total recycle time of 520 ms using 8192 points; 8 dummy scans per t_1 were used for each free induction decay. The total acquisition time was 27 h. The data were processed on a μ-VAX-II station using the FTNMR software written by Dr. Dennis Hare. The time-domain data were multiplied by 30°

phase-shifted sine bell window function in both dimensions. The final data matrix was 2048 × 2048 (complex) over the 43.4 ppm window giving a digital resolution of 7.6 Hz/point, as limited by accessible data arrays.

The phase-sensitive, double-quantum-filtered (DQF-COSY) map shown in portions of Figures 5 and 6 was also collected at 30 °C by standard methods (States et al., 1982; Marion & Wüthrich, 1983). The residual $^1HO^2H$ was suppressed by a 500-ms presaturation pulse (~31 dB) at the end of the relaxation delay. In order to attain the optimal resolution with our available instrumentation, the data were collected over a 7936.5-Hz bandwidth at 500-MHz ^1H frequency, which necessitated restricting the window from 11 to −3 ppm with the transmitter located on the $^1HO^2H$ signals at 4.7 ppm. A total of 256 scans per t_1 [with t_1(max) = 32.3 ms] were collected by using 4096 data points and a 14.7-μs 90° pulse with a total recycle time of 830 ms; 4 dummy scans per t_1 were used for each free induction decay. The total acquisition time was ~34 h. The time-domain data were multiplied by 30° phase-shifted sine bell window function in both dimensions. The final data matrix results in a digital resolution of 3.9 Hz/point, as limited by accessible data arrays.

The nonselective paramagnetic relaxation times for resolved peaks had been determined previously (Cutnell et al., 1981; Ramaprasad et al., 1984a; Unger et al., 1985) and are listed in the tables. Estimates of the paramagnetic T_1s for other protons were derived from the relationship, $T_{1i}/T_{1j} = R_{Fe-i}^{-6}/R_{Fe-j}^{-6}$, where R_{Fe-i} and R_{Fe-j} are the respective distances of protons i and j from the iron. With the known T_{ij} for an assigned proton (heme methyl ~150 ms, R_{Fe-i} ~ 6.1 Å), the remaining T_1s are estimates using R_{Fe-j} from the crystal coordinates of MbCO (Kuriyan et al., 1986). At 7.5 Å, the paramagnetic T_1 is estimated as ~500 ms, which is comparable to expected diamagnetic contributions. Assignment of resonances based on observed NOEs and/or NOESY cross peaks was made on the basis of the internuclear distances obtained from the MbCO crystal structure, at the same time considering the potential paramagnetic relaxation influence on the detected signal, as discussed in detail previously (Emerson et al., 1988). Chemical shifts for all of the spectra were referenced to 2,2-dimethyl-2-silapentane-5-sulfonate (DSS) through the residual water resonance.

Results

The 500-MHz ^1H NMR spectrum of metMbCN in ^2H_2O at 25 °C, pH 8.6, is illustrated in Figure 2A. Resolved peaks are labeled by a letter to denote a residue and a number to indicate the specific proton(s). Previously unambiguously assigned are the heme resonances H5 (5-CH_3), H1 (1-CH_3), H8 (8-CH_3), H2 (2-H_α), H2′ (2-$H_{\beta c}$), and H2″ (2-$H_{\beta t}$) and the amino acid residue signals for Phe CD1, F7 ($C_\zeta H$), F6 ($C_\epsilon Hs$), His E7, D6 ($C_\delta H$), His F8, P3 ($C_\beta H$), His FG3, G6 ($C_\delta H$), and Ile FG5, I4 ($C_\gamma H_3$), I5 ($C_\gamma H$), I6 ($C_\gamma H'$), I7 ($C_\delta H_3$) (Mayer et al., 1974; Ramaprasad et al., 1984a,b; Lecomte & La Mar, 1986; La Mar et al., 1986). The two broad peaks, P8 (19.2 ppm) and P6 (−4.7 ppm), had been tentatively assigned (La Mar et al., 1982) to the proximal His F8 ring protons $C_\delta H$ and $C_\epsilon H$, respectively, on the basis of their large width (~650 Hz), short T_1s (~4 ms), and very similar shifts to the same imidazole protons in model compounds (Chacko & La Mar, 1982). Unassigned are the upfield resolved resonances labeled V2, V4, V5, and T4,L7 (resolved at 30°). The few peaks under the diamagnetic envelope that have been assigned are the heme signals H3 (3-CH_3), H4 (4-H_α), H6 (6-H_α), H6′ (6-H'_α), H7 (7-H_α), and H7′ (7-H'_α) (Sankar et al., 1987; Emerson et al., 1988) and the three amino acid peaks, I3 (Ile FG5 $C_\beta H$), F5 (Phe CD1 $C_\delta Hs$), and P4 [His F8 ($C_\beta H'$) (Ramaprasad et al., 1984b; Lecomte & La Mar, 1986; Emerson et al., 1988)], with chemical shifts as listed in Tables I and II. The mean of the 4-$H_{\beta c}$ and 4-$H_{\beta t}$, but not the individual peaks, was located at −1.1 ppm via heteronuclear decoupling of ^{13}C labels (Sankar et al., 1987). Thus, the four meso-Hs and four propionate H_βs remain unassigned. The 500-MHz ^1H NMR trace in ^1H_2O at 25 °C, pH 8.6, is shown in Figure 3A. In addition to the nonlabile proton signals listed above, three hyperfine-shifted exchangeable proton signals have been identified (Cutnell et al., 1981; Lecomte & La Mar, 1986) on the basis of relaxation and NOEs, His E7 $N_\epsilon H$ (D7), and P1 and P5, the His F8 peptide NH and $N_\delta H$, respectively, as listed in Table II.

The 360-MHz NOESY map for metMbCN in ^2H_2O at 30 °C, pH* 8.6, exhibits only a single weak cross peak between

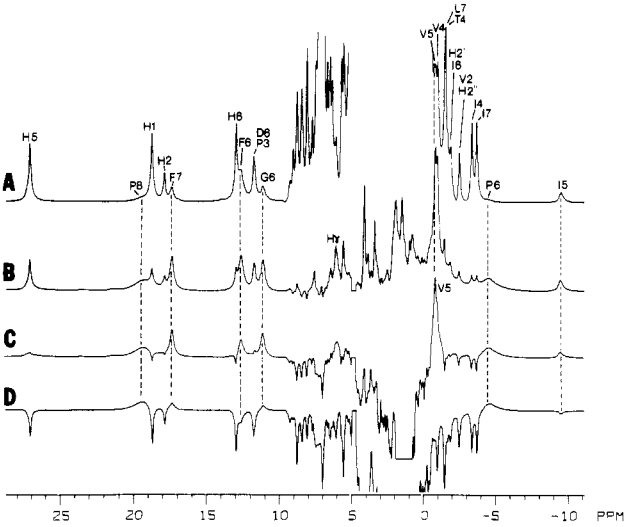

FIGURE 2: 500-MHz ^1H NMR spectra of sperm whale metMbCN in ^2H_2O, pH 8.6, 25 °C. (A) Reference spectrum with residual solvent presaturation collected with a repetition rate of 0.9 s^{-1}. Labeled signals include heme signals (H5 = 5-CH_3, H1 = 1-CH_3, H8 = 8-CH_3; H2 = 2-H_α, H2″ = 2-$H_{\beta t}$; H2′ = 2-$H_{\beta c}$) and amino acid signals (His F8, P8 = ring CH, P3 = $C_\beta H$, P6 = ring CH; Phe CD1, F7 = $C_\zeta H$, F6 = $C_\epsilon Hs$; His E7, D6 = $C_\delta H$; His FG3, G6 = $C_\delta H$; Val E11, V5 = $C_{\gamma 2}H_3$, V4 = $C_{\gamma 1}H_3$; Leu G5, L7 = $C_{\delta 2}H_3$, Thr E10, T4 = $C_\gamma H_3$; and Ile FG5, I5 = $C_\gamma H'$, I4 = $C_\gamma H_3$, I7 = $C_\delta H_3$, I6 = $C_\gamma H'$). (B–D) Inversion–recovery spectra collected under rapid-pulsing conditions to selectively suppress slowly relaxing signals (see Materials and Methods). The acquisition time was 63.5 ms. The delay times (τ) between the composite 180° and 90° pulses were (B) 55 ms, (C) 35 ms, and (D) 15 ms, which resulted in total repetition rates of 8.3, 11.0, and 12.4 s^{-1}, respectively. The relative 3:1 intensity peak V5 to single proton peak P6, P8, or G6 in (C) establishes V5 as a rapidly relaxing methyl with T_1 ~ 20–40 ms.

Table I: Heme Resonance Assignments in MetMbCN

heme proton[a]	peak label	chemical shift[b]	heme proton[a]	peak label	chemical shift[b]
1-CH_3[b]	H1	18.62	6-H'_α	H6′	7.35
3-CH_3[d]	H3	4.76	6-H_β	$H6_\beta$	1.67
5-CH_3[c]	H5	27.03	6-H'_β	$H6_\beta'$	−0.48
8-CH_3[c]	H8	12.88	7-H_α	H7	1.13
2-H_α[e]	H2	17.75	7-H'_α	H7′	−0.45
2-$H_{\beta c}$[e]	H2′	−1.73	7-H_β	$H7_\beta$	1.55
2-$H_{\beta t}$[e]	H2″	−2.55	7-H'_β	$H7_\beta'$	0.78
4-H_α[f]	H4	5.50	α-meso-H	Hα	4.40
4-$H_{\beta c}$	H4′	−1.95	β-meso-H	Hβ	2.09
4-$H_{\beta t}$	H4″	−0.77	γ-meso-H	Hγ	5.98
6-H_α	H6	9.18	δ-meso-H	Hδ	4.09

[a] As labeled in Figure 1. [b] In ppm at 25 °C, pH 8.6. [c] Assignments taken from Mayer et al. (1974). [d] Assignments taken from La Mar et al. (1986). [e] Assignments taken from Ramaprasad et al. (1984a). [f] Assignments taken from Sankar et al. (1987).

Table II: Assignments and Labels for Strongly Relaxed Amino Acid Side-Chain Protons of MetMbCN

residue	position	peak label	chemical shift[a]	R_{Fe}[b]	T_1[c] × 10^{-1} (ms)
IleFG5/99	$C_\alpha H$	12	2.34	8.49	
	$C_\beta H$[d]	13	−0.12	6.79	(28)
	$C_\gamma H_3$[d]	14	−3.46	6.49	20
	$C_\gamma H$[d]	15	−9.60	4.71	6.5
	$C_\gamma H'$[d]	16	−1.91	5.95	12
	$C_\delta H_3$[d]	17	−3.83	6.36	19
Phe	$C_\delta Hs$[e]	F5	8.70	6.86, 8.50	
CD1/43	$C_\epsilon Hs$[e]	F6	12.58	4.67, 6.72	4.7
	$C_\zeta H$[e]	F7	17.27	4.49	2.0
His F8/93	$N_\pi H$[f]	P1	13.20	7.15	
	$C_\alpha H$	P2	7.51	5.94	13
	$C_\beta H$[f]	P3	11.68	6.31	7.5
	$C_\beta H'$[f]	P4	6.43	5.84	(12)
	$C_\delta H$	P6	−4.70	3.33	~0.4
	$N_\delta H$[f]	P5	20.11	5.22	3.0
	$C_\epsilon H$	P8	19.20	3.42	~0.4
His	$C_\beta H$	G3	1.32	6.08	(15)
FG3/97	$C_\beta H'$	G4	−0.48	5.93	(13)
	$C_\delta H$[f]	G6	11.07	4.45	2.1
	$C_\epsilon H$	G8	6.83	7.25	
	$N_\epsilon H$	G7	g	5.39	(7.1)
Val E11/68	$N_\pi H$	V1	g	7.27	
	$C_\alpha H$	V2	−2.55	5.68	11
	$C_\beta H$	V3	1.47	6.40	(20)
	$C_{\gamma 1} H_3$	V4	−1.02	5.10	5.6
	$C_{\gamma 2} H_3$	V5	−0.89	4.14	2-4
His E7/64	$C_\beta H$	D3	3.81	8.72	
	$C_\beta H'$	D4	4.41	8.29	
	$C_\delta H$[f]	D6	11.71	5.89	13
	$C_\epsilon H$	D8	g	4.82	(3.7)
	$N_\epsilon H$[f]	D7	23.7	3.71	1.5

[a] In ppm from DSS, at 25 °C, pH 8.0. [b] Distance from iron, as determined from MbCO X-ray structure (Kuriyan et al., 1986). [c] Experimental T_1 values × 10^{-1} (in ms); calculated values for protons <7.0 Å from iron are given in parentheses. Protons >7.0 Å from the iron would experience negligible paramagnetic relaxation. [d] Assignments taken from Ramaprasad et al. (1984b). [e] Assignments taken from Emerson et al. (1988). [f] Assignments as confirmed by NOEs in Lecomte and La Mar (1986). [g] Not located.

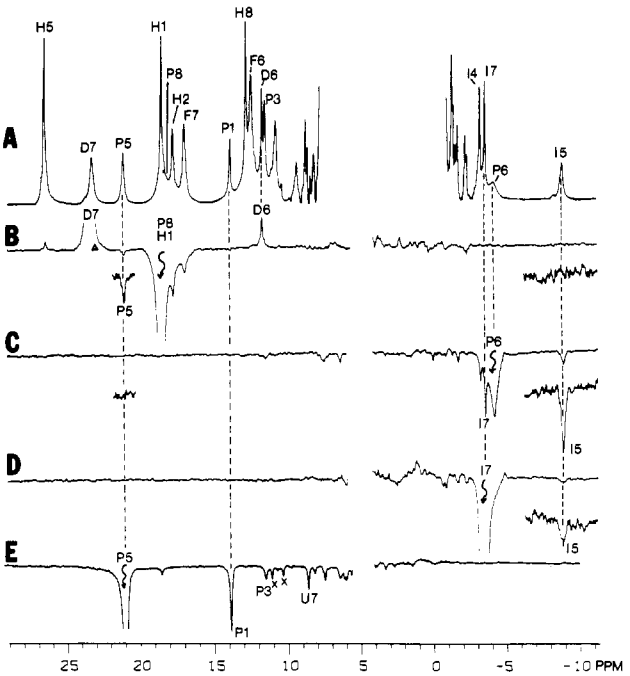

FIGURE 3: 500-MHz ^1H NMR inversion–recovery spectra of metMbCN in ^1H_2O, pH 8.6, 30 °C, collected under rapid-pulsing conditions with a delay time that corresponds to a null for the intense ^1H_2O signal (see Materials and Methods). The time between the 90° observe pulse and the next 180° inversion was 139 ms. The delay between the 180° and 90° pulse (τ) was 385 ms. The 200-ms decoupler presaturation pulse was included in the τ period. The total repetition rate for the acquisition of data was 1.9 s^{-1}. (A) The reference spectrum showing relatively enhanced intensities for faster relaxing signals. Labeled in the spectrum are relevant resonances from heme protons (H5 = 5-CH_3, H1 = 1-CH_3, H8 = 8-CH_3; and H2 = 2-H_α) and amino acid signals (His E7, D7 = $N_\epsilon H$, D6 = $C_\delta H$; His F8, P5 = $N_\delta H$, P8 = $C_\epsilon H$, P1 = $N_\pi H$, P3 = $C_\beta H$, P6 = $C_\delta H$; Phe CD1, F7 = $C_\zeta H$, F6 = $C_\epsilon Hs$; and Ile FG5, I4 = $C_\gamma H_3$, I7 = $C_\delta H_3$, I6 = $C_\gamma H$). (B–E) Difference traces are between one where a selected resonance is saturated and the reference trace with the decoupler placed symmetrical with respect to the resonances for which an NOE is being evaluated (Emerson et al., 1988). The position of the on-resonance decoupler is indicated by a vertical arrow. (B) Saturate H1 (1-CH_3) and P8 (His F8 $C_\epsilon H$) completely; note NOE to P5 (His F8 $N_\delta H$) and the absence of an NOE to Ile FG5 $C_\gamma H$ (peak I5). The positive peaks in (B) are due to partially saturating D7 (His E7 $N_\epsilon H$) [when the decoupler is symmetrical to P5 (indicated by Δ) in the reference trace], as well as the known NOE for D7 to D6 His E7 $C_\delta H$ (Lecomte & La Mar, 1986). The NOE to P5 is not observed when sufficient decoupler power is provided to only saturate the much more slowly relaxing 1-CH_3 (H1) and not the rapidly relaxing His F8 P8. (C) Saturate the rapidly relaxing His F8 peak P6; note NOE to Ile FG5 $C_\gamma H$ peak I5 and the absence of an NOE to His F8 $N_\delta H$ (P5). The Ile FG5 peaks I7 is also weakly off-resonance saturated. (D) Saturate peaks I7 (Ile FG5 $C_\delta H_3$) on-resonance; note much smaller NOE to I5 (Ile FG5 $C_\gamma H$) than when P6 was saturated in (C) above. (E) Saturate His F8 ring $N_\delta H$ (P5); note large NOE to peptide NH (P1), P3, and exchangeable proton signals (marked x), as previously presented by Lecomte & La Mar, (1986), and to nonlabile peak U7.

peaks in the region downfield of 13 ppm [between 1H (1-CH_3) and 2H (2-H_α); not shown]. The off-diagonal section illustrating NOESY cross peaks between the low-field hyperfine-shifted resonances 6–28 ppm and the diamagnetic window 13 to −4 ppm is illustrated in Figure 4. The upper left diagonal portion of the NOESY map upfield of 6.5 ppm is shown in part A of Figure 5, which is combined in the lower right portion (B) with half of the COSY map between 6.5 and −3.0 ppm. A similar split diagonal section of the 8.8–3.6 ppm window NOESY and COSY maps is displayed in the lower right portion A, and the upper left portion B, respectively, of Figure 6. The section of the COSY map shown is determined by the artifacts due to t_1 noise. NOESY peaks will be numbered sequentially in Figure 4 (peaks 1–65), Figure 5 (peaks 66–111), and Figure 6 (peaks 112–118), starting in the lower left of each figure, and identified in the text by the two contributing peaks in parentheses; hence the peak number is a sufficient guide to the appropriate figure displaying the cross peak. For intraresidue cross peaks, we identify the peaks by the standard labeling for amino acid side chains. In the case of interresidue cross peaks, we use the letter/number description for the respective peaks given in Tables I–III. Heme resonances are labeled as shown in Figure 1. A COSY peak, when observed, is designated by the same number as the corresponding NOESY peak, but with an added asterisk. The absence of expected cross peaks in the 2D maps in Figures 4–6 is indicated by a box.

All NOESY cross peaks outside the small portion within 9 to −1.4 ppm shifts were first observed in 1D NOE spectra by saturating the resolved resonance whose better resolution allows clear demonstration of degeneracies in the 2D map due solely to the lower resolution allowable to us (i.e., peaks 18; 23, 24; 29, 30; 32, 33; 38, 39; in Figure 4, and peaks 74; 78; 85, 86; 98; 101, 102; in Figure 5). Thus 82 of the 110 identified 2D cross peaks are observed in 1D spectra, and the chemical shifts of 69 of the 75 assigned resonances can be determined solely from the 1D spectra. Because the 2D map contains all of the NMR data needed to have made the assignments (albeit at lower resolution), we consign representative 1D traces as supplementary material. Also included in the supplementary material are a table identifying the con-

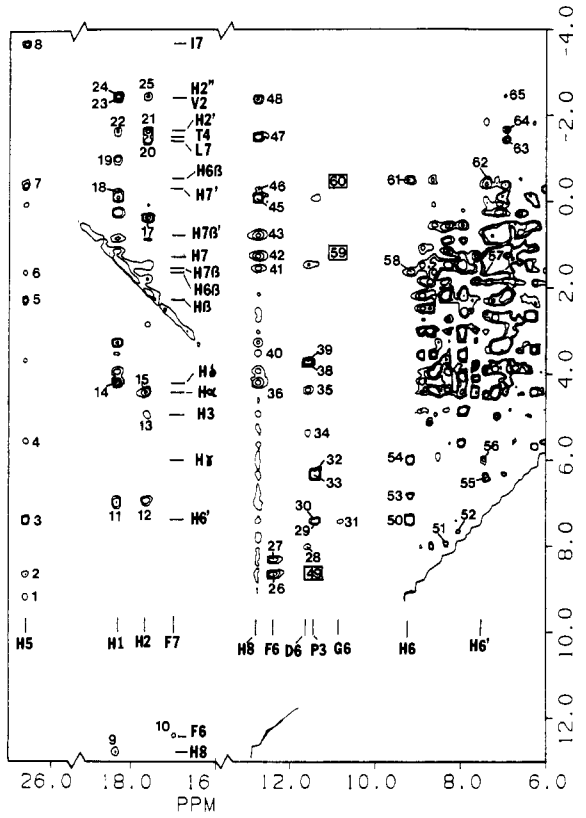

FIGURE 4: A region of the symmetrized 360-MHz ^{1}H phase-sensitive NOESY spectrum of metMbCN, pH 8.6, 30 °C, showing dipolar couplings between the downfield hyperfine-shifted resonances in the 6–28 ppm window and the 13 to −4 ppm range. The counterdiagonal corresponds to the carrier that was positioned at 10.5 ppm to allow optimal digitization over the needed bandwidth. The cross peaks numbered 1–65 correspond to dipolar connectivities described in the text. The correlations between resonance symbols and their respective proton assignments are given in Tables I–III. A number in a solid box indicates the position of an expected NOESY cross peak (based on 1D NOE data) which was not detected. Fifty-seven of the 63 cross peaks (all except 51, 52, 55, 56, and 57) are clearly resolved in variable-temperature 1D NOE experiments. The resonance positions of peaks giving rise to cross peaks in this figure are included in the center. Composite cross peaks readily resolved in 1D NOE traces are 18; 29,30; 32, 33; 38, 39; 45; 46 (see the supplementary material).

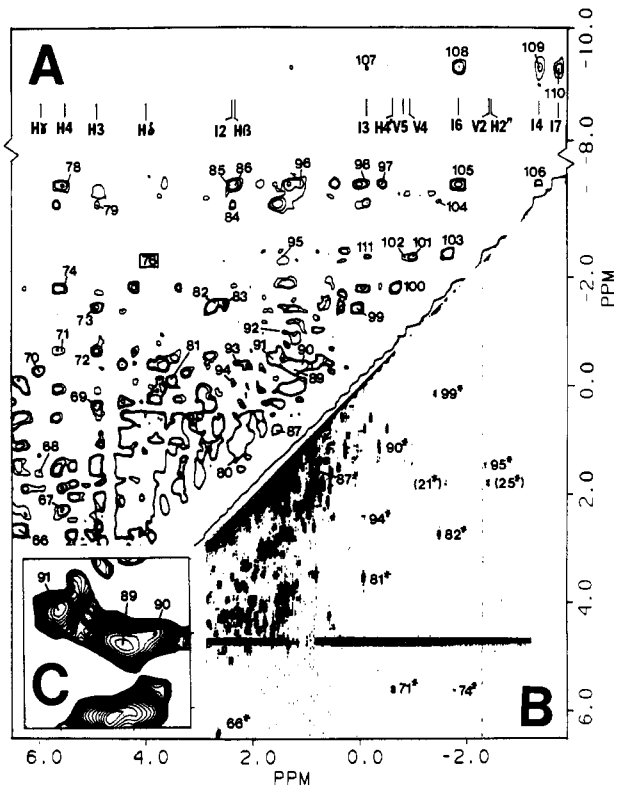

FIGURE 5: Correlation diagram showing (A) upper left portion (6.5 to −4.0 and 6.5 to −10.0 ppm) of the same NOESY spectrum described for Figure 4 and (B) the 6.5 to −3.0 ppm region of a 500-MHz ^{1}H phase-sensitive DQF COSY spectrum of metMbCN, pH 8.6, 30 °C. NOESY cross peaks are numbered 66–111 from the lower left and are described in the text. Identified COSY peaks are labeled by the same number as the corresponding NOESY peak, with an added asterisk. The peaks in parentheses are due to folding back of the 2-H_α peak outside the spectral window. A number in a solid box indicates the position of an expected but unobserved NOESY peak. Inset C at the lower left shows an expanded section of the region involving peaks 89–91 which demonstrates that the individual contributing peaks are readily recognized under better resolution. Twenty-one of the 37 NOESY peaks are clearly resolved in variable-temperature 1D NOE experiments. Composite cross peaks readily resolved in 1D NOE traces are 74; 78; 82, 83; 85, 86; 98; 101, 102. The positions of heme, Ile FG5, and Val E7 peaks contributing to assigned cross peaks are given in the upper portion of (A).

tributing resonance for each cross peak and a schematic representation of the cross peak numbers that connects both intra- and interresidue proton sets.

Heme Resonances. (A) NOESY Peaks. All expected intra-pyrrole NOESY cross peaks between previously assigned resonances are readily detected: 1 (5-CH_3; 6-H_α), 3 (5-CH_3; 6-H′$_\alpha$), 50 (6-H_α; 6-H′$_\alpha$), 42 (8-CH_3; 7-H_α), 46 (8-CH_3; 7-H′$_\alpha$), 89 (7-H_α; 7-H′$_\alpha$), 22 (1-CH_3; 2$H_{\beta c}$), 24 (1-CH_3; 2-$H_{\beta t}$), 103 (2-$H_{\beta c}$; 2-$H_{\beta t}$), 21 (2-H_α; 2-$H_{\beta c}$), and 25 (2-H_α; 2-$H_{\beta t}$). Only very weak dipolar coupling is observed between 2-H_α and 1-CH_3 (not shown). The expected inter-pyrrole contacts, 9 (1-CH_3; 8-CH_3), 13 (2-H_α; 3-CH_3), and 4 (4-H_α; 5-CH_3), are also clearly detected. While only the mean of the 4-$H_{\beta c}$ and 4-$H_{\beta t}$ shifts is known from ^{13}C decoupling experiments (J. S. de Ropp, J. A. McGourty, G. N. La Mar, K. M. Smith, and E. M. Fujinari, manuscript in preparation), the individual 4-H_βs are identified here by observing a pair of NOESY cross peaks to 4-H_α, 74 (4-H_α; 4-$H_{\beta c}$) and 71 (4-H_α; 4-$H_{\beta t}$), whose protons themselves yield the intense cross peak for the geminal 4-H_βs, 100 (4-$H_{\beta c}$; 4-$H_{\beta t}$). Contact between 4-H_βs and 3-CH_3 is clearly observed, 72 (3-CH_3; 4-$H_{\beta t}$); no cross peak is detected between 3-CH_3 and 4-H_α. The unassigned propionate H_βs are identified by the expected cross peaks to the respective known H_αs and the expected intense cross peak between the two H_βs.

For the 6-propionate, the peaks are 58 (6-H_α; 6-H_β), 57 (6-H′$_\alpha$; 6-H_β) at 1.7 ppm and 61 (6-H_α; 6-H′$_\beta$), 62 (6-H′$_\alpha$; 6-H′$_\beta$) at −0.5 ppm [peak is asymmetric with upfield shoulder at 62; peak more clearly seen in 1D NOE of 6-H′$_\beta$ at −0.98 ppm (not shown)], and the intense cross peak 91 (6-H_β; 6-H′$_\beta$); a stronger cross peak to 5-CH_3, 7 (5-CH_3; 6-H′$_\beta$) than 6 (5-CH_3; 6-H_β) places 6-H′$_\beta$ closer to 5-CH_3. The region for the 7-propionate H_βs is too crowded for clear detection at the available resolution (7.6 Hz/point). A pair of peaks with cross peaks to 8-CH_3, 41 (8-CH_3; 7-H_β) and 43 (8-CH_3; 7-H′$_\beta$), themselves exhibit a geminal NOE, 87 (7-H_β; 7-H′$_\beta$). The identity of both 6-H_βs and 7-H_βs was independently confirmed by noting the absence of the NOEs when the propionate β-positions are deuterated (not shown). Three criteria were used to identify the meso-Hs: common cross peaks to the two adjacent pyrrole substituents, line widths of ~70 Hz, and variable temperature intercepts well to the low-field side (10–16 ppm) of the diamagnetic envelope (Thanabal et al., 1987a). Common cross peaks for 5-CH_3 and 4-H_α are 5 (5-CH_3; Hβ) and 67 (4-H_α; H_β) and identify H_β at 2.09 ppm as β-meso-H. Peaks 54 (6-H_α; H_γ), 56 (6-H_α′; H_γ), 68 (6-H_β; H_γ), and 70 (7-H_α; H_γ) assign H_γ at 6.0 ppm to γ-meso-H. Common peaks to 1-CH_3 and 8-CH_3, 14 (1-CH_3; Hδ) and 36

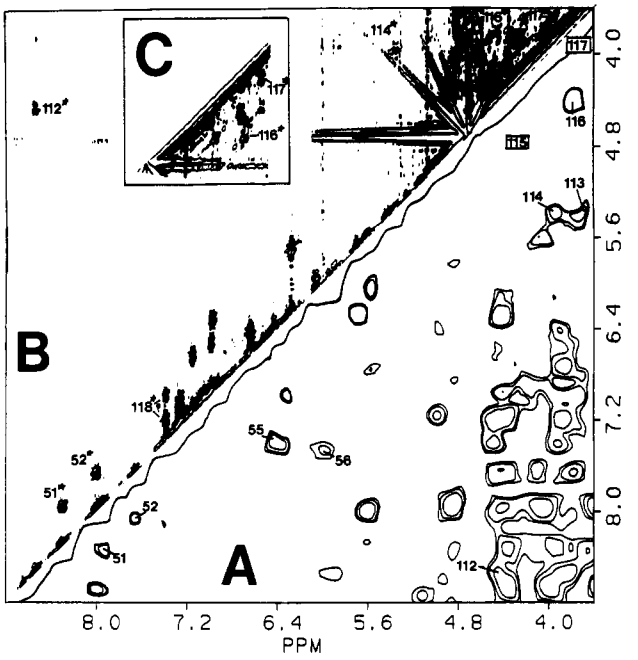

FIGURE 6: Correlation diagram showing (A) lower right portion (8.8–3.6 ppm) of the same 360-MHz ^1H NOESY map of metMbCN in ^2H_2O at 30 °C, pH 8.6, described in Figure 4; new NOESY cross peaks of interest are numbered sequentially 112–118, starting with the lower left, and are described in the text, as well as peaks 51, 52, 55, and 56 already shown in Figure 4. (B) Upper left portion (8.8–3.6 ppm) of the 500-MHz ^1H COSY map of metMbCN in ^2H_2O at 30 °C, pH 8.6; identified COSY cross peaks are numbered the same as the corresponding assigned NOESY peak, with an added asterisk. This section of the map is selected because peak 112* is not obscured by artifacts due to the solvent line. Expected cross peaks which could not be observed are indicated by solid-line boxes. Inset C shows the lower right portion of the COSY map which exhibits fewer artifacts due to the solvent resonance in the region where cross peaks 113*, 116*, and 117* appear.

Table III: Assignments and Labels for Weakly Relaxed Amino Acid Side-Chain Protons in the Heme Pocket of MetMbCN

residue	position	peak label	chemical shift[a]	R_{Fe} (Å)[b]	$T_1 \times 10^{-1}$ (ms)[c]
Leu B10/29	$C_\gamma H$	B5	3.90[d]	8.56	
	$C_{\delta 1}H_3$	B6	3.81	7.98	
	$C_{\delta 2}H_3$	B7	5.53	6.90	(30)
Phe B14/33	$C_\delta Hs$	R5	8.04	10.8, 12.3	
	$C_\epsilon Hs$	R6	8.37	8.57, 10.3	
	$C_\zeta H$	R7	8.40	8.17	
Phe CD4/46	$C_\delta Hs$	Q5	7.69	8.67, 12.6	
	$C_\epsilon Hs$	Q6	8.05	7.64, 11.9	
Thr E10/67	$C_\alpha H$	T2	2.50	9.28	
	$C_\beta H$	T3	2.68	7.24	
	$C_\gamma H_3$	T4	−1.51	7.28	
Ala E14/71	$C_\alpha H$	A2	3.48[d]	9.85	
	$C_\beta H_3$	A3	−0.12	7.41	
Leu F4/89	$C_\alpha H$	U2	[e]	7.19	
	$C_\gamma H$	U5	[e]	6.10	(15)
	$C_{\delta 1}H_3$	U6	[e]	7.49	
	$C_{\delta 2}H_3$	U7	8.71	5.98	(10)
Ala F5/90	$C_\alpha H$	X2	6.50	8.65	
	$C_\beta H_3$	X3	2.63[d]	10.9	
Ser F7/92	$O_\gamma H$	S5	9.71[f]	6.55	(26)
Leu G5/104	$C_\gamma H$	L5	0.07	7.63	
	$C_{\delta 2}H_3$	L7	−1.49	6.00	16
Ile G8/107	$C_\gamma H_3$	E4	0.37	7.66	
	$C_\delta H_3$	E7	[e]	6.17	(16)
Phe H15/138	$C_\delta Hs$	W5	7.05	10.4, 11.2	
	$C_\epsilon Hs$	W6	6.94	7.89, 8.87	
	$C_\zeta H$	W7	7.02	6.96	(33)
Tyr H23/146	$C_\delta Hs$	Y5	7.20 or 7.00[d]	11.8, 12.9	
	$C_\epsilon Hs$	Y6	7.45	9.26, 10.7	

[a] In ppm at 25 °C, pH 8.6, except where indicated otherwise. [b] Distance from the iron from the MbCO X-ray structure (Kuriyan et al., 1986). [c] Nonselective T_1 for proton <7 Å from iron; calculated values, given in parentheses, were not measurable. [d] In ppm at 30 °C, pH 8.6. [e] Not located. [f] Tentative assignments proposed by Lecomte and La Mar (1986).

(8-CH_3; Hδ), determine Hδ as δ-meso-H, and peak 15 (2-H_α; Hα) indicates Hα as the α-meso-H; its expected cross peak to 3-CH_3, 115 (3-CH_3; Hα), is not detectable because Hα is too close to the solvent resonance which is being suppressed. The collective meso-H assignments are again confirmed by noting the absence of the appropriate peaks in 1D NOE spectra (not shown) when using a heme perdeuterated at the four meso positions (La Mar et al., 1980). This locates and unambiguously assigns all 22 heme resonances.

(B) COSY Peaks. Cross peaks are not observed for either 6-H_αs or 7-H_αs, as expected, because of their proximity to the iron ($T_1 \sim 70$ ms, line width ~ 60 Hz). The expected COSY peaks 71* (4-H_α; 4-$H_{\beta t}$) and 74* (4-H_α; 4-$H_{\beta c}$) are observed for the 4-vinyl group because of the large (16- and 10-Hz) couplings; the small 3-Hz $H_{\beta c}$–$H_{\beta t}$ coupling fails to yield a cross peak due to the line width. The 2-vinyl COSY peaks are outside our accessible COSY window. Nevertheless, they are still detected in Figure 5, 21* (2-H_α; 2-$H_{\beta c}$) and 25* (2-H_α; 2-$H_{\beta t}$), folded back as evidenced by their expected shifts. For the propionate H_βs, the 7-H_βs with the much smaller contact shift exhibit a cross peak, 87*, while the more effectively relaxed 6-propionate group H_βs do not. This is likely due to the more efficient relaxation in the latter group by the much larger delocalized spin density (Unger et al., 1985). Thus the COSY map can be expected to allow detection of intra amino acid cross peaks only for pairs of protons >6 Å from the iron due to paramagnetic line width effects. A summary of the heme assignments is given in Table I.

Strongly Relaxed Heme Pocket Residues. The residues possessing the most strongly relaxed protons ($R_{Fe} < 6.0$ Å) are listed in Table II, along with their T_1 values and the distances from the iron (Cutnell et al., 1981; Ramaprasad et al., 1984b; Emerson et al., 1988). Estimated T_1s on the basis of $T_1 \propto R_{Fe}^{-6}$ are given in parentheses for values predicted, 4 ms ($R_{Fe} \sim 3.4$ Å) to 300 ms ($R_{Fe} \sim 7.0$ Å); protons further from the iron will not be dominated by paramagnetic effects. We consider the assignment of individual residues using both NOESY and COSY data, first confirming earlier assignments and then extending them to unassigned protons.

(A) Ile FG5/99. 1D NOEs from $C_\gamma H$ had earlier identified $C_\beta H$, $C_\gamma H'$, $C_\gamma H_3$, and $C_\delta H_3$ (Ramaprasad et al., 1984b). The intraresidue cross peaks expected on the basis of these studies are all observed, 108 ($C_\gamma H$; $C_\gamma H'$), 107 ($C_\gamma H$; $C_\beta H$), 110 ($C_\gamma H$; $C_\delta H_3$), and 109 ($C_\gamma H$; $C_\gamma H_3$), as well as ones that could not be detected by 1D methods, 106 ($C_\gamma H_3$; $C_\delta H_3$), 105 ($C_\gamma H'$; $C_\delta H_3$), and 98 ($C_\beta H$; $C_\delta H_3$) (upfield portion of overlapping two peaks; see the supplementary material). We have previously suggested that the $C_\alpha H$ (I2) peak resonated at −0.2 ppm (Ramaprasad et al., 1984b). However, both NOESY cross peaks 85 (I2; $C_\delta H_3$), 84 (I2; $C_\gamma H_3$), and 94 (I2; $C_\beta H$), and in particular COSY peak 94* (I2; $C_\beta H$), confirm I2 as $C_\alpha H$ at 2.3 ppm. Because of the excessive line widths, COSY peaks are observed only between $C_\alpha H$ and $C_\beta H$, the two protons furthest from the iron. The expected connectivities to the heme are observed, 79 ($C_\gamma H_3$; 3-CH_3), 78 ($C_\delta H_3$; 4-H_α) (high-field shoulder at 78 arises from 4-H_α as confirmed by deuteration on 1D NOE traces; see the supplementary material), 86 ($C_\delta H_3$; γ-meso-H), and 8 ($C_\delta H_3$; 5-CH_3). Small NOEs detectable in 1D studies, but too weak to observe in the NOESY map, are cross peaks between $C_\gamma H$ and 5-CH_3 or 4-H_α.

(*B*) *Phe CD1/43.* The phenyl protons for this rapidly reorienting side chain have been reported on the basis of differential paramagnetic dipolar relaxation and 1D NOEs (Emerson et al., 1988). The NOESY cross peak between $C_\zeta H$ and the rotationally averaged $C_\epsilon Hs$ is observed but is very weak, 10 ($C_\zeta H$; $C_\epsilon Hs$), as expected from the short T_1s (~20 and ~40 ms, respectively). Readily observed is the NOESY peak 26 ($C_\epsilon Hs$; $C_\delta Hs$). The ring proton cross peaks fall outside the spectral window of the collected COSY map. With the available digital resolution, further NOESY peaks to $C_\beta Hs$ and $C_\alpha H$ (all >8 Å from iron) could not be identified in the crowded and poorly digitized diamagnetic region. Connectivities to the heme expected on the basis of earlier 1D NOE studies are $C_\epsilon Hs$ to β-meso-H and 5-CH_3, and $C_\delta Hs$ to 5-CH_3 (Emerson et al., 1988); only the last connectivity could be observed in the NOESY map, 2 ($C_\delta Hs$; 5-CH_3). The remaining cross peaks are too weak to detect.

(*C*) *His F8/93.* Previously unambiguously assigned signals include the ring-labile $N_\delta H$ (P5) and peptide N_pH (P1), $C_\beta H$ (P3), and $C_\beta H'$ (P4) (Cutnell et al., 1981; Lecomte & La Mar, 1986). Tentatively assigned on the basis of comparisons to model compounds are the broad ring protons, $C_\delta H$ (P6) and $C_\epsilon H$ (P8) (La Mar et al., 1982). The intense NOESY cross peak between the geminal H_βs is clearly observed, 32 ($C_\beta H$; $C_\beta H'$) (two components are resolved in 1D NOE traces; see the supplementary material). The common NOEs from the two $C_\beta H$, 29 ($C_\beta H$; P2) and 55 ($C_\beta H'$; P2), together with the cross peak to the previously assigned His FG3 $C_\delta H$, 31 (G6, P2) (Lecomte & La Mar, 1986), identify P2 as $C_\alpha H$ of His F8; COSY peaks are not observed due to the large line widths (~60 Hz for $C_\beta Hs$).

No cross peaks are observed for the broad (~600-Hz), rapidly relaxing proposed His F8 ring protons P6 or P8, in spite of predictions based on the crystal structure that both have close proton neighbors. That P6 and P8 arise from the His F8 ring nonlabile protons is dictated by the fact that only those two protons are close enough to the iron (3.3 Å) to give the observed short T_1s (~4 ms); the question is to which ring positions. The closest dipolar contacts found in the MbCO X-ray structure (Kuriyan et al., 1986) are $C_\epsilon H$ to $N_\delta H$ (peak P5) within His F8, and $C_\delta H$ to Ile FG5 $C_\gamma H$ (I5). Hence, prospects for their assignment are explored by using rapid-pulsing 1D methodology. The trace of metMbCN in ^1H_2O under rapid-pulsing conditions is shown in Figure 3A; the broad peaks with enhanced intensities are P8 under 1-CH_3, and peak P6 on the upfield side of peak I7. The labile His F8 ring proton $N_\delta H$ is P5. Saturation of 1-CH_3 (H1) and the overlapping desired P8 peak is illustrated in the difference trace in Figure 3B; the decoupler in the reference trace is placed symmetrical with respect to P5 ($N_\delta H$), so that any negative intensity for P5 in Figure 3B must represent a true NOE (Emerson et al., 1988). The positive peaks in Figure 3B are due to the fact that peak D7 is saturated in the reference trace, so that both the saturated previously assigned peak D7 (His E7 $N_\epsilon H$) and the peak to which it gives an NOE (D6) appear (Lecomte & La Mar, 1986). Since the NOE to P5 is not observed under low decoupler power where only the slowly relaxing 1-CH_3 is saturated, we can conclude that the NOE to P5 arises from saturating P8 and not 1-CH_3. Thus P8 is consistent with originating from $C_\epsilon H$ and not from $C_\delta H$ of His F8. When previously proposed $C_\epsilon H$ peak P6 is saturated (Figure 3C), a clear NOE is observed to I5 ($C_\gamma H$ of Ile FG5); the reference frequency is symmetrical to I5. While one of the nearby Ile FG5 methyls, I7 ($C_\delta H_3$), is also weakly saturated in Figure 3C, that the NOE to I5 is from saturating P6 is confirmed by detecting a much smaller NOE to I5 when I7 ($C_\delta H_3$) is directly saturated (Figure 3D). *Hence P6 must arise from the $C_\delta H$ rather than $C_\epsilon H$, and the present 1D NOE experiments reverse the previous assignments* (La Mar et al., 1982) *of $C_\delta H$ and $C_\epsilon H$ of the coordinated His F8.* This completes the assignment of all protons of His F8.

(*D*) *His FG3/97.* The only previously assigned peaks are $C_\delta H$ (G6 in Figures 2 and 3), determined on the basis of the extremely short T_1 (~25 ms) and dipolar connectivity to $N_\delta H$ of His F8 in ^1H_2O, and $C_\epsilon H$ (G8), observed upon saturating 6-H_α (Lecomte & La Mar, 1986). No other cross peaks from G6, except that expected to His F8 $C_\alpha H$, 31 (G8; P2), is observed. In the 1D NOE trace (see the supplementary material), however, we observe the two likely $C_\beta H$ peaks at 1.3 and −0.5 ppm whose expected 2D cross peaks we designate 59 (G6; G3) and 60 (G6; G4) in Figure 4. Consistent with the origins of G3 and G4 as the $C_\beta Hs$, we detect an intense NOESY peak 90 (G3, G4) in a very crowded region in Figure 5A (see inset C in Figure 5), but more importantly, we observe the expected COSY peak 90* ($C_\beta H$; $C\beta H'$) in Figure 5B. NOESY connectivities from His FG3 $C_\beta Hs$ to Ile FG5, 96 (G4; I7) and 97 (G3; I7), show which $C_\beta H$ (G3) is closer to Ile FG5. The $C_\alpha H$ was not located. Connectivities to the heme from His FG3 include the expected $C_\beta H$ to β-meso-H, 80 (G3; β-meso-H), 93 (G4; β-meso-H), and $C_\epsilon H$ to 6-H_α 53 (G8; 6-H_α). The remaining labile ring proton could not be located in ^1H_2O (Lecomte & La Mar, 1987), quite possibly because of facile exchange with bulk water.

(*E*) *His E7/64.* Previous assignments include the labile proton signal D7 shown to arise from $N_\epsilon H$ on the basis of both paramagnetic relaxivity and NOEs to the adjacent nonlabile ring proton, $C_\delta H$ (D6) (Cutnell et al., 1981; Lecomte & La Mar, 1986). The expected dipolar couplings from $C_\delta H$ to the two $C_\beta Hs$ (D_3, D_4) are observed, 35 ($C_\delta H$; $C_\beta H$) and 38 ($C_\delta H$; $C_\beta H'$), as supported by both the intense NOESY cross peak 116 ($C_\beta H$; $C_\beta H'$) and corresponding COSY peak 116* ($C_\beta H$; $C_\beta H'$). Neither NOESY nor COSY peaks are expected for the elusive His E7 $C_\epsilon H$ in ^2H_2O (Lecomte & La Mar, 1986). In fact, even 1D NOEs from the labile $N_\epsilon H$ peak in ^1H_2O failed to provide evidence for the location of $C_\epsilon H$, probably because of the expected very rapid relaxation ($T_1 < 35$ ms; $R_{Fe} \sim 4.4$ Å) and its resonance position under the diamagnetic envelope.

(*F*) *Val E11/68.* This is the only functionally critical residue in the heme pocket for which no assignments have been offered to date. There are, however, several as yet unassigned resolved upfield peaks that are candidates for this residue. The single proton peak V2 at −2.6 ppm exhibits a $T_1 \approx 110$ ms, indicating $R_{Fe} \approx 5.9$ Å. This proton also gives NOESY cross peaks to both 1-CH_3, 23 (V2; 1-CH_3), and 8-CH_3, 48 (V2; 8-CH_3). The crystal structure of MbCO (Kuriyan et al., 1986) indicates that there is only one single proton peak ~6 Å from the iron and near both 1-CH_3 and 8-CH_3, Val E11 $C_\alpha H$, to which we assign V2. A weak 1D NOE to the heme δ-meso-H is also seen but is not observed in the NOESY map, 76 (V2; Hδ) (see the supplementary material). Cross peaks from V2 ($C_\alpha H$) are observed to two other upfield peaks, partially resolved peak V5 (−0.9 ppm), 102 (V2; V5), and a resolved methyl peak V4, 101 (V2; V4) ($T_1 \sim 56$ ms, $R_{Fe} \sim 5.2$Å). The intensity of peak V5 and an estimate of its T_1 are established by considering a series of rapid inversion–recovery spectra. Figure 2B–D illustrates the delay times in a modified inversion–recovery experiment using a rapid repetition rate designed to suppress the slowly relaxing diamagnetic envelope so that better effective dynamic range is achieved for observing

broad, fast relaxing signals. In Figure 2D, with τ = 15 ms, only P6 and P8 ($T_1 \sim 4$ ms) are completely relaxed, with F7 ($\sim$20 ms) and G6 ($\sim$25 ms) showing fractional relaxation. Observed in Figure 2C is largely relaxed peak V4 with intensity approximately 3 times that of any of the relaxed single proton peaks P8, F7, G6, and P6; hence V5 has the intensity for a rapidly relaxing methyl peak. The recovery of peak V4 indicates a T_1 in the range 20–40 ms, giving a distance from the iron of 4.4–4.9 Å for methyl V4. At long delays, τ = 55 ms, several other rapidly relaxing signals are detected (Figure 2B), among them Hα, the α-meso-H (estimated $T_1 \approx 65$ ms). Both the short T_1s (and the R_{Fe} derived therefrom) of methyl peaks V4 and V5, as well as their NOESY peaks to $C_\alpha H$ (V2), establish them as the two Val E11 $C_\gamma H_3$s. The Val E11 methyls in the MbCO structure are at 5.5 and 4.5 Å from the iron. The relative T_1 values and NOESY peak between V4 and 1-CH_3 19 (1-CH_3; V4) establish V4 (−1.0 ppm) as $C_{\gamma 1}H_3$ and, hence, V5 as $C_{\gamma 2}H_3$ of Val E11. The Val E11 $C_\beta H$ could not be located unambiguously, although the only common cross peaks from $C_\alpha H$ and $C_\gamma H_3$ at 1.5 ppm (V3), 95 (V3; V2) and 92 (V4; V3), suggest V3 is $C_\beta H$. Given the close proximity to the iron for all Val E11 protons, it is not surprising that COSY peaks could not be detected.

Weakly Relaxed Heme Pocket Amino Acid Residues. With the assignment of all of the heme and above amino acid residue proton signals, it is possible to extend the assignment to several other residues which have some protons <7.5 Å from the iron. Such assignments are pursued on the basis of expected dipolar connectivity as described by the X-ray coordinates and supported by 1D NOE data (see the supplementary material) and COSY and NOESY cross peaks in Figures 4–6. We first locate the closest proton(s) to the assigned protons on the heme and proximal His peripheries by the 1D NOE (see the supplementary material) or 2D NOESY cross peaks as predicted by the X-ray crystal structure (Kuriyan et al., 1986). The nearest neighbor proton(s) scalar coupled to the identified proton(s) is (are) subsequently identifed by the COSY connectivity, as supported by parallel NOESY peaks. No attempt is made at this time to interpret exhaustively the data contained in the two maps, in part because of the low digital resolution available to us.

The two remaining unassigned resolved upfield signals, L7 and T4, are nearly degenerate at 25 °C but diverge at higher temperatures and reveal each peak to have three-proton intensity consistent with the expectation for methyl groups. Methyl T4 ($T_1 \sim 300$ ms, $R_{Fe} \geq 7.3$ Å) gives a strong NOESY peak to 8-CH_3, 47 (T4; 8-CH_3), but none to 1-CH_3, indicating it originates from the nearby (3.3 Å) Thr E10/67 methyl ($R_{Fe} \sim 7.3$ Å). Two cross peaks from T4 at 2.6 ppm, 83 (T4; T2), and 2.8 ppm, 82 (T4; T3), one of which also exhibits a COSY peak 82* (T4; T3), identify T3 as $C_\beta H$ and T2 as the likely $C_\alpha H$ of the same residue. A large common NOESY peak to an apparent methyl peak A3 at 0.12 ppm from both 1-CH_3, 18 (1-CH_3; A3), and 8-CH_3, 45 (8-CH_3; A3), as well as a weaker peak to Val E11 $C_\alpha H$, 111 (A3; V2), uniquely identifies $C_\beta H_3$ of Ala E14/71. A single COSY peak to 3.48 ppm, 81* (A3; A2), together with its NOESY peak, 81 (A3; A2), tentatively locates $C_\alpha H$. The expected weak dipolar coupling for Ala E14 $C_\alpha H$ to the heme, 40 (A2; 8-CH_3), is also observed.

Both pyrrole I substituents exhibit cross peaks at $\sim$7 ppm, 11 (1-CH_3; W), 12 (2-H_α; W), 64 ($2H_{\beta c}$; W), and 65 ($2H_{\beta t}$; W). In better resolved 1D NOE spectra, peak W is composed of peaks at 6.94 (W6) and 7.03 ppm at 25 °C, of which the latter splits into two peaks at higher temperatures, W5 and W7 (see the supplementary material). Since the shifts for W exhibit negligible temperature dependence, they must arise from Phe H15, the only aromatic residue in contact with pyrrole I. Relative intensities of the three components in the 1D NOE spectra upon saturating, 1-CH_3 and 2-H_α, suggest the assignment C_δHs and $C_\zeta H$ at 7.03 ppm and C_ϵHs at 6.94 ppm for the rapidly reorienting ring. Unequivocal is the fact that all three positions resonate at 6.99 ± 0.05 ppm.

The last resolved methyl peak, L7 ($T_1 \sim 160$ ms, $R_{Fe} \approx 6.0$ Å), as well as an apparent methyl peak E4 at 0.37 ppm, exhibits cross peaks to both heme 2-H_α, 20 (L7; 2-H_α) and 17 (E4; 2-H_α), and 3-CH_3, 73 (L7; 3-CH_3) and 69 (E4; 3-CH_3). The X-ray structure identifies two methyls within 3.0 Å of 2-H_α, $C_{\delta 2}H_3$ ($R_{Fe} \sim 6.0$ Å) of proximal Leu G5 and $C_\gamma H_3$ ($R_{Fe} \sim 7.7$ Å) of distal Ile G8. The T_1 value identifies L7 as the former peak, and hence E4 must arise from Leu G5. These assignments are confirmed by a NOESY cross peak from L7 to proximal Phe H15 peak, 63 (L7, W), and a weak cross peak to proximal Ile FG5 $C_\gamma H_3$, 104 (L7; I4). The NOESY, 99 (L5; L7), and COSY, 99* (L5; L7), cross peaks also identify L5 as the $C_\gamma H$ of Leu G5.

The closest contact (3.3 Å) to His E7 $C_\delta H$ (D6) is $C_{\delta 1}H_3$ (B7) of Leu B10, and a strong cross peak, 39 (D6; B7), locates it at 3.81 ppm. The other Leu B10 methyl is $\sim$4 Å from both His E7 $C_\delta H$ and Phe CD1 $C_\zeta H$ and is identified by the common weak NOESY cross peak at 5.5 ppm, 34 (D6; B6), and by the inter-methyl cross peak 113 (B6; B7). A proton at 3.9 ppm that exhibits both NOESY and COSY cross peaks to each of these two methyls, 114 (B5; B7), 114* (B5, B7), and 117* (B5; B6) (the other NOESY expected cross peak 117 is too close to the diagonal to detect), uniquely identifies B5 as $C_\gamma H$ of Leu B10.

Previous 1D NOE studies upon saturating Phe CD1 ring resonances had identified five aromatic protons (via the characteristic intercept) at 8.37 (R6), 8.40 (R7), 8.04 (R5), 8.05 (Q6), and 7.69 (Q5) ppm which must originate form the rapidly reorienting phenyl side chains of Phe B14/33 and Phe CD4/46 (Emerson et al., 1988). COSY peak 51* in Figure 6 connects R6 or R7 and R5. Since the other of R6 or R7 shows no other COSY connectivity, R5, R6, and R7 must arise from one ring, with R5 as C_δHs, and R6 and R7, the nearly degenerate C_ϵHs and $C_\zeta H$. The other two peaks also exhibit a single COSY peak 52*, (Q5, Q6), and no other, indicating that the third position is nearly degenerate with one of the other two. Identification of the aromatic rings is effected by observing the expected NOESY peak from $C_\delta H$ of His E7 to nearby (2.5 Å) Phe CD4 C_ϵHs, 28 (D6; Q6) (better resolved in 1D NOEs; see the supplementary material) which identifies Q6 as C_ϵHs and Q5 as C_δHs or $C_\zeta H$, and hence R5, R6, and R7 as arising from Phe B14. The expected NOESY peak from Phe CD1 C_ϵHs, 27 (F6; R6), identifies R6 as the Phe B14 C_ϵHs.

The remaining residues of interest, Ala F5, Tyr H23, and Leu F4, have dipolar contact primarily with the proximal His F8. A strong 1D NOE is observed to peak U7 at 8.6 ppm upon saturating the exchangeable His F8 $N_\delta H$ (P5), as illustrated in part E of Figure 3. Varying the solvent isotope composition reveals U7 is nonlabile, and variable temperature data reveal a very strong temperature dependence, with the peak becoming partially resolved on the low-field side of the envelope at 0 °C and exhibiting apparent three-proton intensity. A weaker NOE to U7 is also seen when saturating either His F8 peptide NH (P1) or $C_\beta H$ (P3) (not shown). The crystal coordinates place a single group in the proximity of these three His F8 protons, the $C_{\delta 2}H_3$ of Leu F4. The strong temperature de-

pendence reflects the very substantial downfield hyperfine shift experienced by this methyl group. The His F8 C_βHs make two additional close dipolar contact to Tyr H23/146 C_ϵH (3.1 Å) and Ala F5/90 C_αH (3.0 Å), and relevant NOESY peaks are 30 (P3; Y6) at 7.45 ppm and 33 (P3; X2) at 6.4 ppm. The shift for Y6 is essentially independent of temperature and hence arises from rapidly reorienting (Dalvit & Wright, 1987) Tyr H23 C_ϵHs, while that of X2 moves strongly upfield at higher temperatures and must originate in Ala F5 C_αH. There are two COSY peaks from 7.45 ppm (Y6) to 7.20 and 7.00 ppm, one of which, 118* (Y6; Y5), must be the Tyr rotationally averaged C_δHs (Y5). The Ala F5 C_αH peak exhibits both a NOESY, 66 (X2; X3), and COSY peak, 66* (X2; X3), which uniquely identify X3 as the Ala F5 $C_\beta H_3$ at 2.63 ppm. The available assignments of the more distant amino acid residues are listed in Table III.

Discussion

Scope and Limitations of 2D Experiments. The NOESY map of metMbCN exhibits detectable cross peaks for the majority of the NOEs observed in steady-state 1D NOE experiments and allows assignment of most of the resonances of interest. It is also obvious that many more small, largely redundant NOEs are observed in the 1D NOE traces (Ramaprasad et al., 1984a,b; Emerson et al., 1988; see also figures in supplementary material) which are not critical to assignment. The failure to observe the rest of the expected peaks in the 2D map is largely due to sensitivity problems which are, in part, due to the limitation of the accessible spectrometer and, in part, due to the inherently reduced NOESY peak intensities in paramagnetic systems. Another limitation of the present NOESY data, in comparison with parallel 1D NOE data, is the low resolution allowed by our data system. Both of these problems, however, can be overcome with better instrumentation and do not constitute inherent limitations of the NOESY data. Very strongly relaxed and extremely broad (~600-Hz) protons which may not exhibit NOESY peaks even under ideal conditions are shown to exhibit dipolar connectivity sufficient to allow unambiguous assignment using 1D NOE measured under rapid-pulsing conditions. It is noted that, of the total of 75 identified proton signals, the shifts and at least some major dipolar connectivities of all but 6 (labeled with superscript *d* in Table III) could be observed solely by 1D NOE methodology. This provides both some calibration of the 2D NOESY map as well as support for the utilization of 1D NOEs in conjunction with 2D maps.

The DQF-COSY map was found uninformative for all protons closer than ~6 Å, due to both the rapid relaxation and increased line width. It is likely that a rotating-frame correlation experiment (not accessible on our instrumentation) which gives only positive cross peaks [i.e., TOCSY or HOHAHA (Braunshweiler & Ernst, 1983; Bax & Davis, 1986)] may provide the needed additional scalar connectivities for some of the intermediate line width peaks. Nevertheless, the observation of clear COSY cross peaks in unusual spectral windows in ^2H_2O (i.e., peaks 66* and 112*) not common to diamagnetic systems demonstrates that spin connectivities can be followed even for strongly hyperfine-shifted resonances provided they experience only weak paramagnetic relaxation. It is also obvious that, due to variable relaxation contributions from the iron, a number of sophisticated 2D experiments that can be routinely implemented for an analogous diamagnetic complex (i.e., MbCO), such as RELAY or spin filtering (Dalvit & Wright, 1987), may not provide the definitive information desired for hyperfine-shifted peaks of a paramagnetic derivative. Hence, it is likely that 2D methods cannot provide the complete solution structure of a paramagnetic protein by sequence-specific assignments in a fashion now attainable for diamagnetic molecules (Wüthrich, 1986). On the other hand, the distance dependence from the iron for the paramagnetic relaxivity ($T_1 \propto R_{Fe}^{-6}$) provides an additional structural probe invaluable for identifying precisely those resonances least likely to benefit from the 2D NMR methodologies (Ramaprasad et al., 1984b; Lecomte & La Mar, 1986; Emerson et al., 1988). The present work clearly demonstrates that, at least in principle, complete assignment of resonances of a paramagnetic protein is possible with 2D NMR methodologies, particularly when supplemented by 1D NOE and paramagnetic relaxivity data, providing good X-ray structural data are available to identify the expected dipolar contacts. Hence we consider the prospects for resonance assignments and structure determination of at least low-spin ferric hemoproteins very encouraging.

Status of Assignments. Fifty new resonances have been assigned to add to the 28 previously identified peaks; 22 of the total are the complete assignment of the heme, with distances from the iron ranging from ~4.5 (meso-Hs) to ~7.5 Å (vinyl H_βs). There are a total of 31 nonequivalent amino acid proton sets ≤7.0 Å from the iron, with ~90% clearly assigned, 25 of the 27 nonlabile and 3 of the 4 labile protons, leaving only His E7 C_ϵH (4.8 Å), Ile G8 $C_\delta H_3$ (6.2 Å), and the labile His FG3 N_ϵH (5.4 Å) mising. The labile His FG3 proton likely is exchanging with the solvent. Extending the sphere to 7.5 Å adds 9 protons, 6 of which are assigned (85% assigned with $R_{Fe} < 7.5$ Å); among the missing 3 is another labile proton, Val E11 N_pH, and two Leu F4 signals. Moreover, 20 signals from protons >7.5 Å have also been identified. It is clear that even the present 2D map may provide additional assignments, although better digitized maps, particularly as a function of temperature, are required for an optimal assignment strategy. The available assignments, however, emphasize the desired proximity to the iron and provide the necessary input data for developing a quantitative understanding of the shifts in terms of detailed electronic (contact shift) and magnetic (dipolar shift) properties of the active site.

Active Site Molecular/Electronic Structure. The detection of strong NOESY cross peaks only between the methyl and the adjacent vinyl H_βs and not H_α on the same pyrrole establish largely cis configurations for the two vinyls, as found both in the crystal structures (Takano, 1977; Phillips, 1980; Kuriyan et al., 1986) and by NMR in MbCO (Mabbutt & Wright, 1985). The hyperfine shift pattern for the heme, which is known to be largely contact in nature, is similar to that in related model compounds except for the larger asymmetry (Shulman et al., 1971; La Mar, 1979; La Mar & Walker, 1979; Satterlee, 1985). The last heme substituent assignments confirm that the shifts are larger for all substituents on pyrroles I and III than pyrroles II and IV. The meso-H hyperfine shifts are all very similar, 4.1 ± 2.0 ppm, and do not show strong alternate biases upfield and downfield for adjacent positions as found, for example, in ferricytochrome b_5 (McLachlan et al., 1988). This small spread of the meso-H hyperfine shifts is consistent with either negligible rhombic dipolar shifts or an in-plane magnetic axis which passes close to N–Fe–N vectors (Thanabal et al., 1987a). We show in our companion report that the latter is clearly the case (Emerson & La Mar, 1990).

The present assignment by 1D NOEs of the two His F8 nonlabile ring protons contradicts earlier ones based on models (La Mar et al., 1982). The axial imidazole shifts in the ap-

propriate monoimidazole, monocyano heme model complex have been unequivocally established by isotope labeling, with $C_\epsilon H$ at 2 ppm and $C_\delta H$ at 14 ppm (Chacko & La Mar, 1982). MetMbCN exhibits two His F8 ring signals with shifts similar to those in the model but with interchanged assignments. Thus the similarity in shifts is fortuitous. Such a discrepancy in hyperfine shift pattern between model and protein is unprecedented and suggests much greater caution in using models for such assignments in proteins without some confirmatory experiments (La Mar & Walker, 1979; La Mar, 1979). The pattern of the coordinated His ring proton hyperfine shift has been proposed to serve as a useful indicator of the degree of imidazolate character (La Mar et al., 1982; Thanabal et al., 1987b). The similarity of the His F8 ring shifts in model and protein was used to infer the absence of significant hydrogen-bond donation by the His F8 imidazole side chain to a backbone carbonyl in Mb (La Mar et al., 1982). The present reassignments clearly negate such simple conclusions. This interpretation may still be valid for the low-spin ferric horseradish peroxidase complex, where 1D NOE studies unequivocally established the individual proximal His ring proton assignments (Thanabal et al., 1987b). The significant changes in His F8 hyperfine shift between model and metMbCN are obviously an indicator of protein-induced perturbation(s) on the heme electronic/magnetic/molecular structure and provide important information on the influence of protein constraints on ligation. In our companion report (Emerson & La Mar, 1990), we utilize the presently determined assignments to develop a quantitative understanding of the hyperfine shifts in metMbCN which resolves the difference between protein and model in terms of distal steric tilting of the bound cyanide ligand.

Acknowledgments

We are indebted to C. Yu for assistance with preliminary 2D NOESY experiments and J. S. de Ropp and S. J. McLachlan for useful discussions.

Supplementary Material Available

Figures 1–4, showing 1D NOE difference traces upon saturating all resolved resonances of metMbCN in ^2H_2O, with NOEs labeled by the corresponding cross peak number in the text, and providing the improved resolution that allows characterization of individual peaks found degenerate in the 2D NOESY map, Figure 5, giving a schematic representation identifying intra- and interresidue cross peaks, and Table I, giving a sequential identification of cross peak numbers by contributing residues (6 pages). Ordering information is given on any current masthead page.

References

Antonini, E., & Brunori, M. (1971) *Hemoglobin and Myoglobin in Their Reactions with Ligands*, North-Holland, Amsterdam.

Bax, A., & Davis, D. G. (1986) *J. Magn. Reson. 65*, 355–360.

Braunschweiler, L., & Ernst, R. R. (1983) *J. Magn Reson. 53*, 521–528.

Case, D. A., & Karplus, M. (1978) *J. Mol. Biol. 123*, 697–701.

Chacko, V. P., & La Mar, G. N. (1982) *J. Am. Chem. Soc. 104*, 7002–7007.

Cutnell, J. D., La Mar, G. N., & Kong, S. B. (1981) *J. Am. Chem. Soc. 103*, 3567–3572.

Dalvit, C., & Wright, P. E. (1987) *J. Mol. Biol. 194*, 313–327.

Debrunner, P. G., & Frauenfelder, J. (1982) *Ann. Rev. Phys. Chem. 33*, 283–299.

Eads, T. M., Kennedy, S. D., & Bryant, R. G. (1986) *Anal. Chem. 58*, 1752–1756.

Emerson, S. D., & La Mar, G. N. (1990) *Biochemistry* (following paper in this issue).

Emerson, S. D., Lecomte, J. T. J., & La Mar, G. N. (1988) *J. Am. Chem. Soc. 110*, 4176–4182.

Gelin, B. R., Lee, A. W., & Karplus, M. (1983) *J. Mol. Biol. 171*, 489–559.

Horrocks, W. D., Jr. (1973) in *NMR of Paramagnetic Molecules* (La Mar, G. N., Horrocks, W. D., Jr., & Holm, R. H., Eds.) pp 127–177, Academic Press, New York.

Jesson, J. P. (1973) in *NMR of Paramagnetic Molecules* (La Mar, G. N., Horrocks, W. D., Jr., & Holm, R. H., Eds.) pp 1–52, Academic Press, New York.

Karplus, M., & McCammon, A. D. (1981) *CRC Crit. Rev. Biochem. 9*, 293–349.

Krishnamoorthi, R., La Mar, G. N., Mizukami, H., & Romero, A. E. (1984) *J. Biol. Chem. 259*, 8826–8831.

Kumar, N. V., & Kallenbach, N. R. (1985) *Biochemistry 24*, 7658–7662.

Kuriyan, J., Wilz, S., Karplus, M., & Petsko, G. A. (1986) *J. Mol. Biol. 192*, 133–154.

La Mar, G. N. (1973) in *NMR of Paramagnetic Molecules* (La Mar, G. N., Horrocks, W. D., Jr., & Holm, R. H., Eds.) pp 86–157, Academic Press, New York.

La Mar, G. N. (1979) in *Biological Applications of Magnetic Resonances* (Shulman, R. G., Ed.) pp 305–342, Academic Press, New York.

La Mar, G. N., & Walker, F. A. (1979) in *The Porphyrins* (Dolphin, D., Ed.) Part IVB, pp 61–159, Academic Press, New York.

La Mar, G. N., Budd, D. L., Smith, K. M., & Langry, K. C. (1980) *J. Am. Chem. Soc. 102*, 1822–1823.

La Mar, G. N., de Ropp, J. S., Chacko, V. P., Satterlee, J. D., & Erman, J. E. (1982) *Biochim. Biophys. Acta 708*, 317–325.

La Mar, G. N., Emerson, S. D., Lecomte, J. T. J., Pande, U., Smith, K. M., Craig, G. W., & Kehres, L. A. (1986) *J. Am. Chem. Soc. 108*, 5568–5573.

Lecomte, J. T. J., & La Mar, G. N. (1985) *Biochemistry 24*, 7388–7395.

Lecomte, J. T. J., & La Mar, G. N. (1986) *Eur. Biophys. J. 13*, 373–382.

Mabbutt, B. C., & Wright, P. E. (1985) *Biochim. Biophys. Acta 832*, 175–185.

Macura, S. R., & Ernst, R. R. (1980) *Mol. Phys. 40*, 95–117.

Marion, D., & Wüthrich, K. (1983) *Biochem. Biophys. Res. Commun. 113*, 962–974.

Mayer, A., Ogawa, S., Shulman, R. G., Yamane, T., Cavaleiro, J. A. S., Rocha Gonsalves, A. M. d'A., Kenner, G. W., & Smith, K. M. (1974) *J. Mol. Biol. 86*, 749–756.

McLachlan, S. J., La Mar, G. N., & Lee, K.-B. (1988) *Biochim. Biophys. Acta 957*, 430–445.

Noggle, J. H., & Shirmer, R. E. (1971) *The Nuclear Overhauser Effect*, Academic Press, New York.

Patt, S. L., & Sykes, B. D. (1972) *J. Chem. Phys. 56*, 3182–3184.

Perutz, M. F. (1989) *Trends Biochem. Sci. (Pers. Ed.) 14*, 42–44.

Phillips, S. E. V. (1980) *J. Mol. Biol 142*, 531–554.

Ramaprasad, S., Johnson, R. D., & La Mar, G. N. (1984a) *J. Am. Chem. Soc. 106*, 3632–3635.

Ramaprasad, S., Johnson, R. D., & La Mar, G. N. (1984b) *J. Am. Chem. Soc. 106*, 5330–5335.

Sankar, S. S., La Mar, G. N., Smith, K. M., & Fujinari, E. M. (1987) *Biochim. Biophys. Acta 912*, 220-229.
Satterlee, J. D. (1985) *Annu. Rep. NMR Spectrosc. 17*, 79-178.
Shulman, R. G., Glarum, S. H., & Karplus, M. (1971) *J. Mol. Biol. 57*, 93-115.
Springer, B. A., Egeberg, K. D., Sligar, S. G., Rohlfs, J. M., & Olson, J. S. (1989) *J. Biol Chem. 264*, 3057-3060.
States, D. J., Haberkorn, R. A., & Ruben, D. J. (1982) *J. Magn. Reson. 48*, 286-292.
Swift, T. J. (1973) in *NMR of Paramagnetic Molecules* (La Mar, G. N., Horrocks, W. D., Jr., & Holm, R. H., Eds.) pp 53-83, Academic Press, New York.
Takano, T. (1977) *J. Mol. Biol. 110*, 537-568.
Thanabal, V., de Ropp, J. S., & La Mar, G. N. (1987a) *J. Am. Chem. Soc. 109*, 265-272.
Thanabal, V., de Ropp, J. S., & La Mar, G. N. (1987b) *J. Am. Chem. Soc. 109*, 7516-7525.
Thanabal, V., de Ropp, J. S., & La Mar, G. N. (1988) *J. Am. Chem. Soc. 110*, 3027-3035.
Unger, S. W., Jue, T., & La Mar, G. N. (1985) *J. Magn. Reson. 61*, 448-456.
Williams, G., Moore, G. R., Porteous, R., Robinson, M. N., Soffe, N., & Williams, R. J. P. (1985a) *J. Mol. Biol. 183*, 409-428.
Williams, G., Clayden, N. J., Moore, G. R., & Williams, R. J. P. (1985b) *J. Mol. Biol. 183*, 447-460.
Wüthrich, K. (1986) *NMR of Proteins and Nucleic Acids*, Wiley, New York.
Wüthrich, K., Shulman, R. G., Yamane, T., Wyluda, B. J., Hügli, T. E., & Gurd, F. R. N. (1970) *J. Biol. Chem. 245*, 1947-1953.

NMR Determination of the Orientation of the Magnetic Susceptibility Tensor in Cyanometmyoglobin: A New Probe of Steric Tilt of Bound Ligand†

S. Donald Emerson and Gerd N. La Mar*
Department of Chemistry, University of California, Davis, California 95616
Received June 6, 1989; Revised Manuscript Received September 11, 1989

ABSTRACT: The experimentally determined paramagnetic dipolar shifts for noncoordinated amino acid side-chain protons in the heme pocket of sperm whale cyanometmyoglobin [Emerson, S. D., & La Mar, G. N. (1990) *Biochemistry* (preceding paper in this issue)] were used to determine in solution the orientation of the principal axes for the paramagnetic susceptibility tensor relative to the heme iron molecular coordinates. The determination was made by a least-squares search for the unique Euler rotation angles which convert the geometric factors in the molecular (crystal) coordinates to ones that correctly predict each of 41 known dipolar shifts by using the magnetic anisotropies computed previously [Horrocks, W. D., Jr., & Greenberg, E. S. (1973) *Biochim. Biophys. Acta 322*, 38-44]. An excellent fit to experimental shifts was obtained, which also provided predictions that allowed subsequent new assignments to be made. The magnetic axes are oriented so that the z axis is tipped $\sim 15°$ from the heme normal toward the heme δ-meso-H and coincides approximately with the characterized FeCO tilt axis in the isostructural MbCO complex [Kuriyan, J., Wilz, S., Karplus, M., & Petsko, G. A. (1986) *J. Mol. Biol. 192*, 133-154]. Since the FeCO and FeCN units are isostructural, we propose that the dominant protein constraint that tips the magnetic z axis from the heme normal is the tilt of the FeCN by steric interactions with the distal residues. The rhombic magnetic axes were found to align closely with the projection of the proximal His imidazole plane on the heme, confirming that the His-Fe bonding provides the protein constraint that orients the in-plane anisotropy. The tipped magnetic z axis is shown to account quantitatively for the previously noted major discrepancy between the hyperfine shift patterns for the bound imidazole side chain in models and protein. Moreover, it is shown that the proximal His ring nonlabile proton hyperfine shifts provide direct and exquisitely sensitive indicators of the degree of the z axis tilt that may serve as a valuable probe for characterizing variable steric interactions in the distal pocket of both point mutants and natural genetic variants of myoglobin.

The inherently high information content of the hyperfine-shifted resonances of low-spin ferric hemoproteins has long been recognized, and extensive NMR studies of both model compounds and various hemoproteins have been reported (Wüthrich, 1970; Shulman et al., 1971; La Mar, 1979; La Mar & Walker, 1979; Satterlee, 1985). These hyperfine shift patterns are highly sensitive to systematic perturbations as found in closely related natural genetic variants and synthetic point mutants of myoglobin (Mb)[1] and contain key information on the modulation of chemical reactivity by the nature of the polypeptide chain (Wüthrich et al., 1970; Krishnamoorthi et al., 1984; Satterlee, 1985; Springer et al., 1989). The full exploitation of this information, however, has to date been prevented because of the inability to unambiguously assign the heme pocket residue peaks and to quantitatively separate the dipolar and contact contributions to the observed hyperfine shift (Jesson, 1973; Horrocks, 1973; Bertini & Luchinat, 1986):

$$\delta_{hf} = \delta_{con} + \delta_{dip} \quad (1)$$

† This research has been supported by a grant from the National Institutes of Health (HL 16087).

[1] Abbreviations: Mb, myoglobin; Hb, hemoglobin; metMbCN, cyanide-complexed ferric Mb; NMR, nuclear magnetic resonance; DSS, 2,2-dimethyl-2-silapentane-5-sulfonate; ESR, electron spin resonance.

0006-2960/90/0429-1556$02.50/0